


Anastasis Drives Senescence and Non-Cell Autonomous Neurodegeneration in the Astrogliaopathy Alexander Disease

Liqun Wang,¹ Hassan Bukhari,¹ Linghai Kong,^{2,3} Tracy L. Hagemann,² Su-Chun Zhang,^{2,3}  Albee Messing,^{2,4} and Mel B. Feany¹

¹Department of Pathology, Brigham and Women's Hospital, Harvard Medical School, Boston, Massachusetts 02115, ²Waisman Center, University of Wisconsin-Madison, Madison, Wisconsin 53705, ³Department of Neuroscience and Department of Neurology, School of Medicine and Public Health, University of Wisconsin-Madison, Madison, Wisconsin 53705, and ⁴Department of Comparative Biosciences, School of Veterinary Medicine, University of Wisconsin-Madison, Madison, Wisconsin 53705

Anastasis is a recently described process in which cells recover after late-stage apoptosis activation. The functional consequences of anastasis for cells and tissues are not clearly understood. Using *Drosophila*, rat and human cells and tissues, including analyses of both males and females, we present evidence that glia undergoing anastasis in the primary astrogliaopathy Alexander disease subsequently express hallmarks of senescence. These senescent glia promote non-cell autonomous death of neurons by secreting interleukin family cytokines. Our findings demonstrate that anastasis can be dysfunctional in neurologic disease by inducing a toxic senescent population of astroglia.

Significance Statement

Under some conditions cells otherwise destined to die can be rescued just before death in a process called anastasis, or “rising from the dead.” The fate and function of cells undergoing a near death experience is not well understood. Here, we find that in models and patient cells from Alexander disease, an important brain disorder in which glial cells promote neuronal dysfunction and death, anastasis of astrocytic glia leads to secretion of toxic signaling molecules and neurodegeneration. These studies demonstrate a previously unexpected deleterious consequence of rescuing cells on the brink of death and suggest therapeutic strategies for Alexander disease and related disorders of glia.

Introduction

Anastasis was initially described in cultured cells exposed to chemical toxins that recovered from late-stage apoptosis. The recovery process was named from the Greek word for resurrection

from death (Tang et al., 2012). Anastasis has been best defined in cell culture systems where multiple hallmarks of late-stage cell death can be assessed and the morphologic, cell biological and molecular characteristics of cells can be followed over time. Anastasis has also been described *in vivo*. In particular, transgenic markers of anastasis based on the ability to mark cells with prior activation of executioner caspases have been engineered and used to describe anastasis during development and in response to cellular stress in *Drosophila* (Tang et al., 2015; Ding et al., 2016). However, the role of anastasis in tissue and organismal health is unclear, with both positive and negative roles proposed (Sun and Montell, 2017; Tang and Tang, 2018).

Here, we study the role of anastasis in models of Alexander disease, a rare and severe disorder characterized by seizures and leukodystrophy in infants and brainstem and spinal cord dysfunction and atrophy in older individuals (Messing et al., 2012). Both early and late onset cases are characterized neuropathologically by the deposition of abundant eosinophilic, beaded proteinaceous inclusions, termed Rosenthal fibers, in affected brain tissue. Rosenthal fibers are highly enriched in the astrocytic intermediate filament glial fibrillary acidic protein (GFAP; Goldman and Corbin, 1988;

Received Aug. 14, 2021; revised Oct. 4, 2021; accepted Oct. 29, 2021.

Author contributions: L.W. and M.B.F. designed research; L.W., H.B., L.K., T.L.H., and M.B.F. performed research; T.L.H., S.-C.Z., and A.M. contributed unpublished reagents/analytic tools; L.W., H.B., S.-C.Z., and M.B.F. analyzed data; H.B., L.K., T.L.H., S.-C.Z., A.M., and M.B.F. edited the paper; L.W. and M.B.F. wrote the paper.

This work was supported by the NIH-NICHD Grant P01HD076892, the Intellectual and Developmental Disabilities Research Centers at Boston Children's Hospital (NIH-NICHD Grant U54HD090255), and the Waisman Center (NIH-NICHD Grant U54HD090256). Fly stocks obtained from the Bloomington *Drosophila* Stock Center (NIH Grant P40OD018537), the Vienna *Drosophila* Resource Center, D. Williams, N. Bouchon, and H. Jiang were used in this study. We thank the Transgenic RNAi Project (TRiP) at Harvard Medical School [National Institutes of Health (NIH)-National Institute of General Medical Science Grant R01GM084947] for making transgenic RNAi stocks. Monoclonal antibodies were obtained from the Developmental Studies Hybridoma Bank developed under the auspices of the National Institute of Child Health and Human Development (NICHD) and maintained by the University of Iowa, Department of Biology, Iowa City, IA, and the UC Davis/NIH NeuroMab Facility. Human tissue was obtained from the NICHD Brain and Tissue Bank for Developmental Disorders at the University of Maryland, Baltimore, MD. Kit Tuen and Yi Zhong provided excellent technical assistance.

The authors declare no competing financial interests.

Correspondence should be addressed to Mel B. Feany at mel_feany@hms.harvard.edu.

<https://doi.org/10.1523/JNEUROSCI.1659-21.2021>

Copyright © 2022 the authors

Johnson and Bettica, 1989; Heaven et al., 2016). GFAP is even more directly linked in the pathogenesis of Alexander disease because dominant missense mutations in the *GFAP* gene cause the disorder. The presence of protein aggregates formed by a protein critical for disease pathogenesis puts Alexander disease firmly in the category of protein aggregation-related neurologic disorders (Hartl, 2017). Indeed, increasing molecular chaperones has substantial benefit in experimental models of the disease (Koyama and Goldman, 1999; Hagemann et al., 2009; Wang et al., 2011).

However, Alexander disease is unique in that aggregates are found exclusively in glia, correlating with the predominant astrocytic expression of GFAP. Since significant loss of neurons and oligodendroglial cells characterizes the neuropathology of early and late onset Alexander disease patients (Brenner et al., 2009; Messing et al., 2012), the disorder represents an important exemplar of a primary astrogliaopathy and a unique opportunity to dissect experimentally the mechanisms governing non-cell autonomous toxicity in central nervous system disease. While glial influences are increasingly understood to be important in a widening variety of human neurologic diseases, in most disorders it remains challenging to dissect the primary importance of neuronal versus glial pathology in disease pathogenesis.

The unequivocal association of dominant missense mutations in GFAP with clinical Alexander disease has motivated successful modeling of the disorder in multiple *in vivo* systems. Expression of disease-linked mutant GFAP in mice, including in knock-in models, induces a Nrf2-dependent cellular stress response accompanied by robust Rosenthal fiber formation (Hagemann et al., 2006, 2012). Similarly, flies expressing mutant GFAP in glia accumulate numerous Rosenthal fiber-like inclusions, mediated through protein aggregation and oxidative stress and accompanied by glial apoptosis and non-cell autonomous neuronal death (Wang et al., 2011). More recently, Hagemann and Messing have described rats with knock-in of GFAP^{R237H}, orthologous with the severe GFAP^{R239H} human mutation (Hagemann et al., 2021). These knock-in rats in addition to showing robust aggregation of mutant GFAP into Rosenthal fibers also display motor impairment and spinal cord atrophy. Finally, a variety of cellular models have been described based on expression of disease-associated GFAP in cultured astrocytes. Human astrocytes derived from Alexander disease patients have been particularly useful in replicating cellular features of the human disease (Jones et al., 2018; Wang et al., 2018). Here, we use fly, rat and iPSC models, together with analysis of postmortem human tissue, to suggest a toxic role for anastasis affecting Alexander disease astrocytes through development of cellular senescence.

Materials and Methods

Drosophila stocks and genetics

All fly crosses were performed at 25°C; adults were aged at 29°C to increase transgene expression. The genotype of the *Drosophila* model of Alexander disease is: *repo-GAL4*, *UAS-GFAP^{R79H}/+* (GFAP^{R79H} for simplicity in the manuscript). Control is *repo-GAL4/+*. The *repo-GAL4* driver mediates expression in a pan-glial pattern. Genetic manipulations mediated by *repo-GAL4* are therefore specific to glia. Loss of function genetic reagents (*Df(3L)H99*, *dome^{G0441}*) were used in the heterozygous state and reduce target gene expression globally. The pan-neuronal driver *elav-GAL4* mediates specific neuronal gene knock-down. The QUAS expression system and the pan-glial *repo-QF2* driver was used in experiments using the anastasis reporter and manipulation of neuronal gene expression by *GAL4*. The following stocks were obtained from the Bloomington *Drosophila* Stock Center: *repo-GAL4*, *elav-GAL4*, *UAS-p35*, *Df(3L)H99*, *UAS-dome RNAi* (TRIP.HMJ21208), *dome^{G0441}*, *Ubi-CasExpress*, *G-trace* (Bloomington #28 280). The *upd3-lacZ* line was

obtained from N. Buchon and H. Jiang. D. Williams kindly provided the *UAS-CD8-PARP-Venus* line. C. Potter provided *repo-QF2* flies.

Human samples

Frozen frontal cortex from five controls (mean age 10 years, range 1–27 years; two females and three males) and six Alexander disease patients (mean age eight years, range 1–27 years; three females and three males) were obtained from the NICHD Brain and Tissue Bank for Developmental Disorders at the University of Maryland, Baltimore, MD. GFAP mutations in the Alexander disease patients included R79C (14 years), R239C (7 years), R239H (two cases; both 1 year), K63E (27 years), and one uncharacterized (1 year). All cases had typical neuropathology of Alexander disease, including multiple Rosenthal fibers. Postmortem intervals were comparable between cases and controls and were <24 h in all cases. For immunostaining analysis tissue was thawed and fixed in 4% paraformaldehyde overnight before paraffin embedding.

Rats

AxD model rats were generated using CRISPR/Cas9 mutagenesis to produce a R237H mutation in the endogenous rat *Gfap* gene (Hagemann et al., 2021), and animals were backcrossed into the CD (Sprague Dawley) IGS background (Charles River) for four generations. Both male and female eight-week-old heterozygous *Gfap^{+/R237H}* rats were used for experiments and sex-matched and age-matched wild-type littermates were used as controls. Animals were euthanized by CO₂ asphyxiation, brains harvested and bisected at the midline, with one half microdissected and frozen (−80°C) for molecular analysis and the other half immersion fixed in 4% paraformaldehyde for histologic analysis. All experiments were approved by the College of Letters and Sciences and Vice Chancellor's Office for Research and Graduate Education Animal Care and Use Committee at the University of Wisconsin–Madison.

iPS cells and astrocyte differentiation

Alexander disease iPS cells were made from fibroblasts from a patient carrying the R88C mutation in GFAP (Jones et al., 2018). The corrected control line was made via CRISPR/Cas9 gene editing (Jones et al., 2018). Astrocytes were differentiated using a previously described protocol (Jones et al., 2018). The cells were checked for mycoplasma every three to four months and were free of mycoplasma contamination. The cells were also morphologically consistent under microscope examination.

Immunohistochemistry, immunofluorescence, and terminal deoxynucleotidyl transferase biotin-dUTP nick end labeling (TUNEL) analysis

For immunostaining, adult flies were fixed in formalin and embedded in paraffin; 4-μm serial frontal sections were prepared through the entire fly brain and placed on a single glass slide. In some studies, whole mount *Drosophila* brain preparations were alternatively used. Rat and human samples were fixed in 4% paraformaldehyde, embedded in paraffin and sectioned at a thickness of 6 μm. Rat and human tissue used for senescence-associated β-galactosidase staining was cryosectioned at 6-μm thickness. Astrocytes differentiated from iPS cells were also fixed in 4% paraformaldehyde before proceeding to immunostaining.

For immunostaining, paraffin slides were processed through xylene, ethanol, and into water. Antigen retrieval by boiling in sodium citrate, pH 6.0, was performed before blocking. Slides were blocked in PBS containing 0.3% Triton X-100 and 2% milk for 1 h and then incubated with appropriate primary antibodies overnight. Primary antibodies used were: anti-Elav (9F8A9, Developmental Studies Hybridoma Bank) at 1:5; anti-HP1α (C1A9, Developmental Studies Hybridoma Bank) at 1:50; anti-HP1α (2616, Cell Signaling) at 1:50; anti-β-galactosidase (z3781, Promega) at 1:500; anti-p53 (H3, Developmental Studies Hybridoma Bank) at 1:5; anti-p53 (FL-393, Santa Cruz) at 1:500; anti-pH2Av (Rockland) at 1:100; anti-pH2Ax (2577, Cell Signaling) at 1:50; anti-cleaved human PARP (E51, Abcam) at 1:10,000; anti-GFP (N86/8, NeuroMab) at 1:5; anti-GFAP (Z0334, DAKO) at 1:5000; anti-GFAP (N206/8, NeuroMab) at 1:500; anti-Repo (8D12, Developmental Studies Hybridoma Bank) at 1:5; anti-IL-6 (ab9324, Abcam) at 1:50; anti-IL-6 (D3K2N, Cell Signaling) at 1:50; rabbit monoclonal anti-p21 (12D1, Cell Signaling) at 1:50. For immunohistochemistry, biotin-conjugated secondary antibodies (1:200, SouthernBiotech) and avidin-biotin-

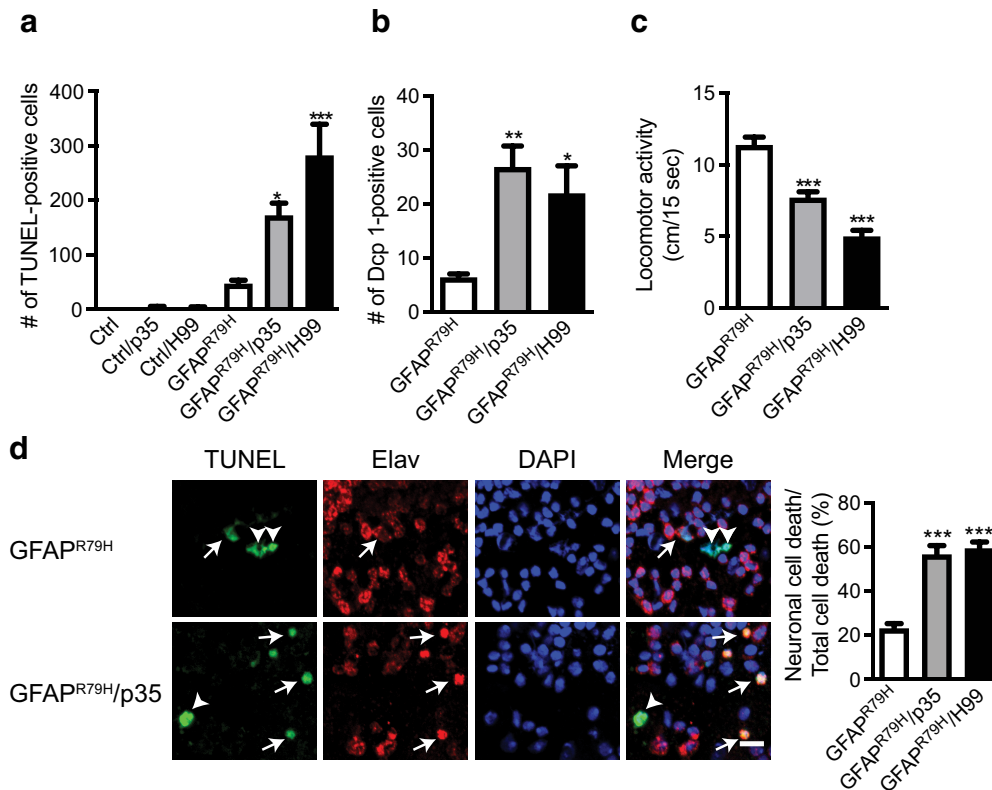


Figure 1. Inhibition of glial caspase activity induces neuronal cell death in Alexander disease model flies. **a**, Genetic inhibition of caspase activity in glial cells increases the number of apoptotic cells in Alexander disease model flies. $N \geq 6$ per genotype. $*p < 0.01$, $***p < 0.0001$. **b**, Genetic inhibition of caspase activity in glial cells increases the number of Dcp-1 (Death caspase-1)-positive cells in Alexander disease model flies. $N \geq 6$ per genotype. $*p < 0.05$, $**p < 0.01$. **c**, Genetic inhibition of caspase activity in glial cells reduces locomotor activity in Alexander disease model flies. $N \geq 18$ per genotype. $***p < 0.0001$. **d**, Double label immunofluorescence shows increased neuronal cell death (arrows) in Alexander disease model flies with caspase inhibition in glial cells. Arrowheads indicate non-neuronal apoptotic cells. Scale bar: 5 μ m. Quantification is shown in the right panel. $N \geq 6$ per genotype. $***p < 0.001$. One-way ANOVA with multiple comparison analysis. Control (Ctrl): *repo-GAL4/+*. GFAP^{R79H}: *repo-GAL4, UAS-GFAP^{R79H}/+*. Flies are 20 d old. Extended Data Figure 1-1 is supporting this figure.

peroxidase complex (Vectastain Elite, Vector Laboratories) staining was performed using DAB (Vector Laboratories) as a chromagen. For immunofluorescence studies, appropriate Alexa Fluor-conjugated secondary antibodies (Alexa 488, Alexa 555, or Alexa 647; 1:200, Invitrogen) were used. In some experiments, tyramide amplification (ThermoFisher) was used to increase the fluorescence signal. All immunostaining data were replicated in at least three animals and representative images are shown. ELISA was also used to assay IL-6 levels in rat tissue using the V-PLEX Proinflammatory 2 Rat kit from Meso Scale Discovery.

Apoptotic cell death was visualized using TUNEL labeling according to manufacturer's instructions (TdT FragEL DNA fragmentation kit, Calbiochem), with Alexa 488-conjugated streptavidin (Invitrogen).

SenTraGor was obtained from Arriani Pharmaceuticals and was used following the protocol supplied. Senescence-associated β -galactosidase activity was assayed following fixation in 2% paraformaldehyde and 0.2% glutaraldehyde using a histochemical staining kit from Sigma (CS0030). Cells and tissues were fixed for 6–7 min, incubated with X-gal staining solution at 37°C for 16 h and mounted in aqueous mounting medium.

Western blottings

Human (white matter from frontal cortex) and rat (corpus callosum and hippocampus) samples were prepared and homogenized in RIPA buffer (50 mM Tris, 150 mM NaCl, 0.1% SDS, 0.5% deoxycholate, 1% NP40, pH 7.4, with protease inhibitor cocktail, ThermoFisher Scientific) and centrifuged at $14,000 \times g$ for 15 min at 4°C. Supernatant was used for Western blottings. *Drosophila* brains were homogenized in 1 \times Laemmli buffer (Sigma). All samples were boiled for 10 min at 100°C, briefly centrifuged and subjected to SDS-PAGE using 10% or 4–12% gels (Lonza). Proteins were transferred to nitrocellulose membranes (Bio-Rad),

blocked in 2% milk in PBS with 0.05% Tween 20, and immunoblotted with primary antibodies. Primary antibodies used were anti-MMP1 (3A6B4, 3B8D12, Developmental Studies Hybridoma Bank) at 1:100; anti-HP1 α (C1A9, Developmental Studies Hybridoma Bank) at 1:1000; anti- β -galactosidase (z3781, Promega) at 1:10,000; anti-p53 (H3, Developmental Studies Hybridoma Bank) at 1:100; anti-pH2Av (Rockland) at 1:2000; anti-p21 (EPR3993, Abcam) at 1:3000; anti-p21 (12D1; Cell Signaling) at 1:500; anti-Phospho-p53 (Ser15; 9284, Cell Signaling) at 1:1000; anti-pH2Ax (2577, Cell Signaling) at 1:2500; anti-GAPDH (MA5-15738, ThermoFisher Scientific) at 1:100,000; anti-actin (JLA20, Developmental Studies Hybridoma Bank) at 1:4000; anti-GFP (N86/6, NeuroMab) at 1:500; anti-cleaved caspase-3 (ab13847, Abcam) at 1:2000. The appropriate horseradish peroxidase-conjugated secondary antibody (1:20,000, SouthernBiotech) was applied and signal was detected with West Femto chemiluminescent substrate (ThermoFisher Scientific). Images were taken using a FluorChem HD2 system (ProteinSimple). All blots were repeated at least three times, and representative blots are shown in the figures. Western blottings were quantified using NIH ImageJ software and statistical analysis was performed using unpaired *t* test (two samples) or one-way ANOVA with Tukey's multiple comparison test (three or more samples). Each data point represents mean \pm SEM.

Behavioral analysis

Flies were collected in fresh vials on the day of eclosion and were transferred to fresh vials every 3 d. The locomotor assay was performed on day 20. To count the number of centimeters walked in 15 s, a single fly was tapped gently to the same initial starting position in its vial and the vial was placed over a gridded surface. The number of centimeters traversed was counted four times per fly,

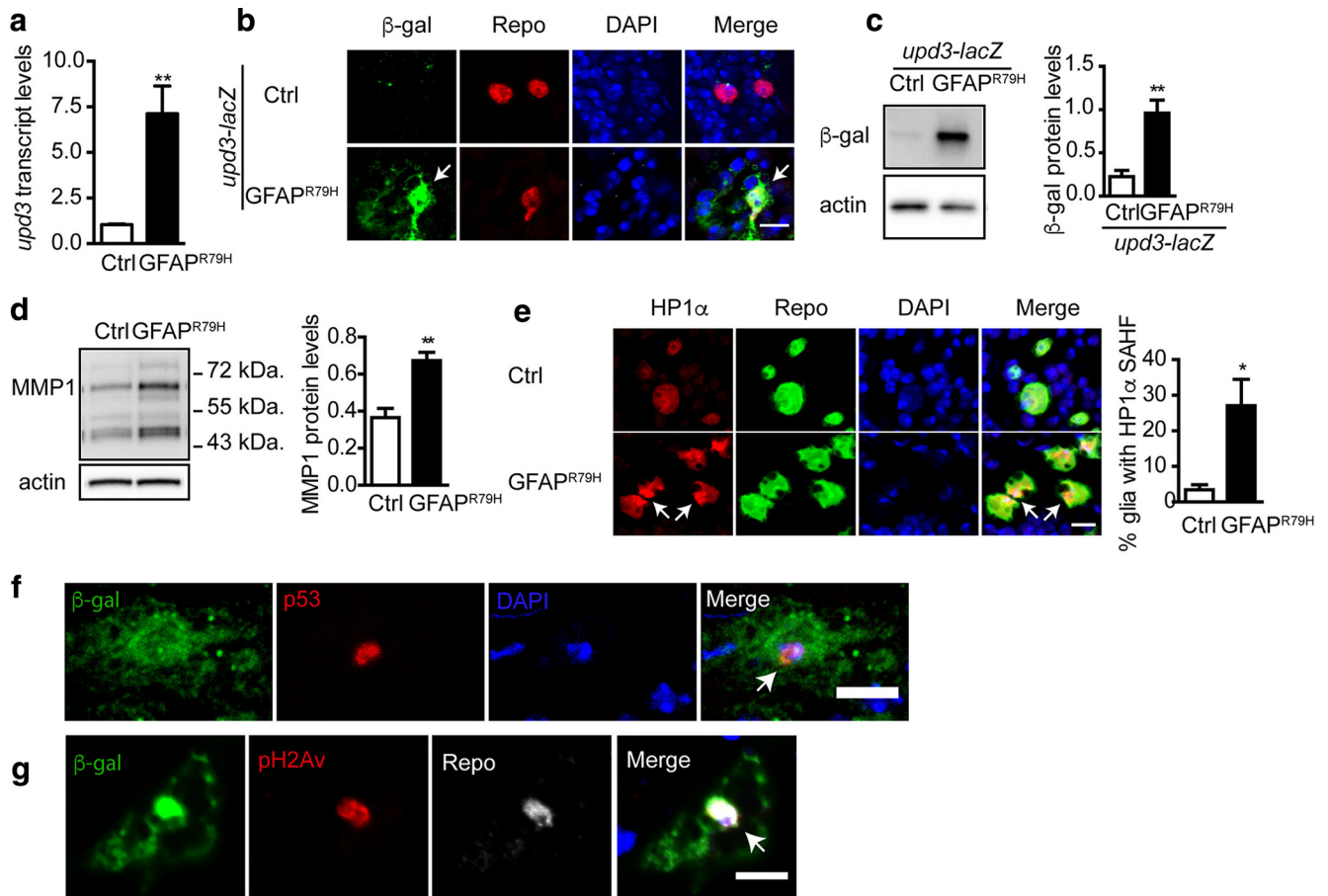


Figure 2. Glial cells in GFAP transgenic flies express markers of senescence. **a**, Increased *upd3* transcript level in GFAP transgenic flies compared with age-matched control flies. $N \geq 6$. $**p < 0.01$, unpaired *t* test. **b**, Double label immunofluorescence shows β -galactosidase expression of the *upd3-lacZ* in glia of GFAP transgenic flies (arrow), but not in age-matched controls. Repo marks glial cells. DAPI labels nuclei. Scale bar: 5 μ m. **c**, Western blotting demonstrates a marked increase of β -galactosidase expression (*upd3-lacZ*) in GFAP transgenic flies compared with age-matched controls. $N = 4$. $**p = 0.0046$, unpaired *t* test. **d**, Western blotting demonstrates a significant increase of MMP1 expression in GFAP transgenic flies compared with age-matched controls. $N = 4$. $**p = 0.0036$, unpaired *t* test. Blots were reprobed with an antibody to actin to illustrate equivalent protein loading. **e**, Double label immunofluorescence shows increased formation of senescence-associated HP1 α heterochromatin foci (SAHF) in GFAP transgenic flies (arrows, bottom panel) compared with age-matched controls. Repo marks glial cells. DAPI labels nuclei. Scale bar: 5 μ m. Quantification is in the right panel. $N = 5$ for control and 6 for GFAP^{R79H}. $p = 0.0184$, unpaired *t* test. **f**, Double label immunofluorescence shows colocalization of β -galactosidase (*upd3-lacZ*) and p53 in GFAP transgenic flies (arrow). Scale bar: 5 μ m. Genotype: *repo-GAL4*, *UAS-GFAP^{R79H}*, *upd3-lacZ/+*. **g**, Double label immunofluorescence shows colocalization of β -galactosidase (*upd3-lacZ*) and pH2Av in GFAP transgenic flies (arrow). Scale bar: 5 μ m. Genotype: *repo-GAL4*, *UAS-GFAP^{R79H}*, *upd3-lacZ/+*. Ctrl: *repo-GAL4/+*. GFAP^{R79H}: *repo-GAL4*, *UAS-GFAP^{R79H}*. Flies are 20 d old.

and at least 18 flies of each genotype were assayed. Equal numbers of female and male flies were assayed.

Confocal microscopy

Fluorescent images were taken using confocal microscopy: Leica SP8 X confocal microscope, Harvard NeuroDiscovery Center Enhanced Neuroimaging Core facility, Olympus Fluoview 1000 confocal microscope, Harvard Medical School Neurobiology Imaging facility, or a Zeiss LSM-800 confocal microscope with Airyscan. For the quantification of cultured Alexander disease astrocytes, coverslips containing both control and patient derived cells were scanned to obtain a tile image by using the Tile Scan Module included in Zen Blue software of the LSM-800 confocal microscope. The image contained a resolution of 0.1 μ m/pixel and was acquired with a Plan-Apochromat 20 \times /0.8 M27 objective. A grid of squares was manually added to the tile scan image and positive cells were quantified within each square by using ImageJ software. Imaging parameters, including pinhole, laser power, detector gain, and pixel dwell time were the same between control and Alexander disease astrocytes.

Real-time PCR

RNA was isolated from 20-d-old *Drosophila* brains (16 brains per sample) using QIAzol (QIAGEN) and reverse-transcribed with the High-Capacity

cDNA Reverse Transcription kit (Applied Biosystems) according to the manufacturer's instruction. Real-time PCR was performed and monitored using SYBR Green PCR Master Mix (Applied Biosystems) in a StepOnePlus Real-Time PCR system (Applied Biosystems) according to manufacturer's instructions. *Drosophila* ribosomal protein Rpl32 was used as a control. Each data point represents the mean \pm SEM.

Primers: *upd3*: 5'-CCGGCTGACCTTCCAGC-3'; 5'-ATCCTTTGGCGTTTCTTGCA-3' and *Rpl32*: 5'-GACCATCCGCCAGCATAC-3'; 5'-CGGCGACGCACTCTGTT-3'.

Statistical analysis

Statistical analysis was performed using GraphPad Prism 5 software. Each data point represents mean \pm SEM. Unpaired *t* test was used for comparison of two groups. One-way ANOVA with Tukey's multiple comparison test was used for comparison of three groups or more. The χ^2 test was used for seizure behavior analysis.

Results

We have previously described a *Drosophila* model of Alexander disease based on expression of disease-linked forms of mutant human GFAP in fly glia. Our model recapitulates key features of the human disorder, including GFAP aggregation and non-

cell autonomous neurodegeneration. Based on TUNEL staining and cell counts there is also a modest, but reproducible, amount of glial cell death (Wang et al., 2011, 2015). To determine whether death of glia contributes to secondary neurodegeneration we blocked glial cell apoptosis in transgenic flies expressing R79H mutant human GFAP in glia using the pan-glial *repo-GAL4* driver. We either co-expressed the baculovirus antiapoptotic protein p35 (Hay et al., 1994) or made flies heterozygous for the H99 deletion, which removes the proapoptotic genes *reaper*, *hid*, and *grim* (Chen et al., 1996). Surprisingly, rather than reducing neuronal death both anti-apoptotic reagents markedly increased cell death in the brains of flies expressing mutant human GFAP in glia as assessed by TUNEL staining (Fig. 1*a*) or caspase activation (Fig. 1*b*). Increased cell death was accompanied by worsened locomotor dysfunction (Fig. 1*c*). To determine the cell type(s) affected by blocking glial apoptosis we co-stained brain tissue sections for TUNEL (Fig. 1) or activated caspase (Extended Data Fig. 1-1) and the neuronal (*elav*) or glial (*repo*) nuclear markers. We found that, as we have reported previously (Wang et al., 2015, 2016, 2018), both neurons (Fig. 1*d*, arrows; Extended Data Fig. 1-1*a*, arrows) and glia (Fig. 1*d*, arrowhead; Extended Data Fig. 1-1*a*, arrows) degenerate when mutant GFAP is expressed in glia. Blocking glial apoptosis produces a striking increase in non-cell autonomous neuronal death (Fig. 1*d*).

To ensure that our anti-apoptotic reagents were working as expected we expressed a transgenic caspase reporter in which the extracellular and transmembrane domain of mouse CD8 is fused to 40 amino acids from human PARP, including the caspase cleavage site (UAS-CD8-PARP-Venus; Williams et al., 2006) using the *repo-GAL4* glial driver. We observed a significant upregulation of the caspase reporter when we expressed mutant human GFAP, as monitored by immunostaining (Extended Data Fig. 1-1*c*) or Western blotting (Extended Data Fig. 1-1*d*) with an antibody specific for cleaved human PARP. As expected, transgenic expression of p35 or heterozygosity for the H99 deletion significantly reduced caspase activation using the transgenic reporter expressed in glial cells (Extended Data Fig. 1-1*e*). We performed Western blot analysis to ensure that p35 expression or haploinsufficiency for H99 did not affect transgenic GFAP levels (Extended Data Fig. 1-1*f*).

The unexpected non-cell autonomous effect of preventing glial programmed cell death is reminiscent of the “undead” phenomenon in which blocking apoptosis leads to compensatory

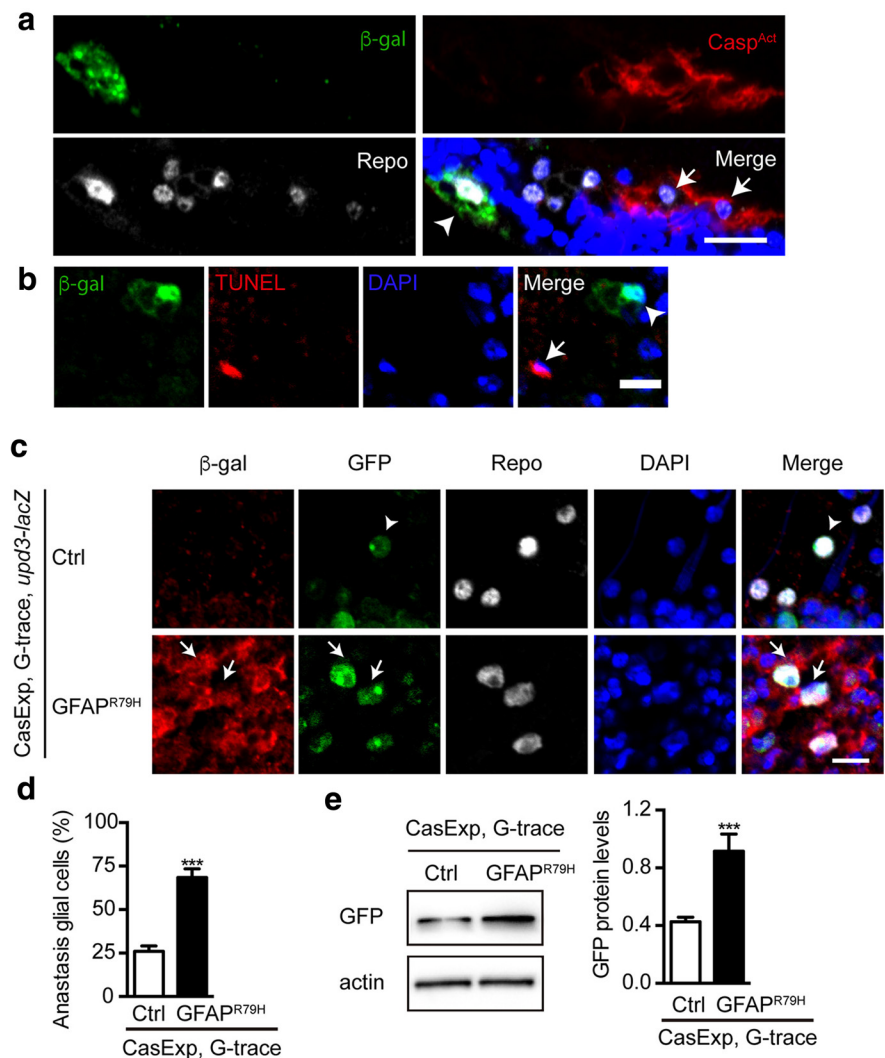


Figure 3. Anastasis in Alexander disease model glia. *a*, Double label immunofluorescence shows β -galactosidase (*upd3-lacZ*)-positive cells (arrowhead) do not colocalize with active caspase-positive cells (CD8-PARP-Venus reporter, arrows). Scale bar: 5 μ m. Genotype: *repo-GAL4*, UAS-GFAP^{R79H}, *upd3-lacZ*/UAS-CD8-PARP-Venus. Flies are 20 d old. *b*, Double label immunofluorescence shows β -galactosidase (*upd3-lacZ*)-positive cells (arrowhead) do not colocalize with TUNEL-positive cells (arrow). Scale bar: 5 μ m. Genotype: *repo-GAL4*, UAS-GFAP^{R79H}, *upd3-lacZ*/+. Flies are 20 d old. *c*, Immunofluorescence staining shows β -galactosidase (*upd3-lacZ*)-positive cells colocalize with glial cells showing anastasis (GFP-positive cells, arrows) in GFAP transgenic flies. Arrowhead shows activation of the anastasis reporter in control flies. Scale bar: 5 μ m. *d*, Quantification shows a marked increase of anastasis-positive glial cells in GFAP transgenic flies compared with age-matched controls. $N = 6$ per genotype, *** $p < 0.0001$, unpaired t test. Flies are 30 d old. *e*, Western blotting demonstrates increased anastasis marked by GFP expression in GFAP transgenic flies compared with age-matched controls. $N = 4$, *** $p < 0.0001$, unpaired t test. The blot was reprobed with an antibody to actin to illustrate equivalent protein loading. Flies carrying the anastasis reporter are heterozygous for the CasExp transgene (*Ubi-CasExpress/+*) and the G-trace reporter (Evans et al., 2009). Flies are 30 d old.

proliferation through secretion of growth factors (Pérez-Garijo et al., 2004; Martín et al., 2009). We thus wondered whether blocking glial cell apoptosis might prolong glia in a toxic secretory state in Alexander disease. We therefore assessed the activity of major secretory signaling pathways, including cytokines (Vanha-Aho et al., 2016), in our mutant human GFAP transgenic flies. We observed significant upregulation of the *Drosophila* cytokine *upd3* using quantitative real time PCR (Fig. 2*a*). We then co-labeled brain sections for markers of glia and neurons and a well-characterized *upd3-lacZ* reporter (Zhou et al., 2013) and observed upregulation of *upd3* in glial cells in Alexander disease model flies (Fig. 2*b*, arrows, *c*).

Since elevated cytokine release is a feature of cellular senescence (Neves et al., 2015) we assessed other markers of

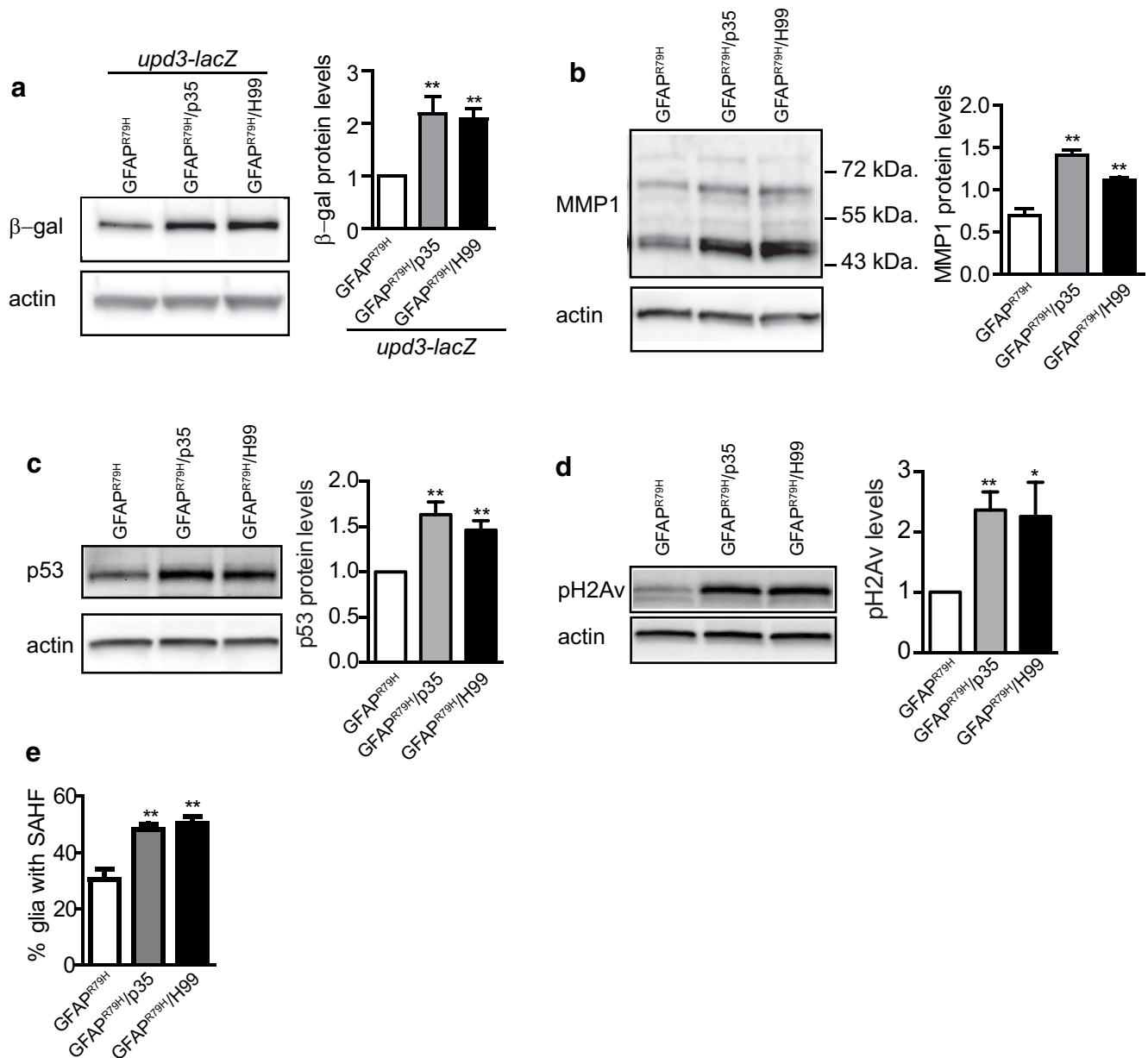


Figure 4. Inhibition of glial caspase activity promotes senescence in Alexander disease model flies. **a**, Genetic inhibition of glial caspase activity increases β -galactosidase expression (*upd3-lacZ*) in GFAP transgenic flies. $N = 5$. ** $p < 0.01$. **b**, Genetic inhibition of glial caspase activity markedly increases MMP1 protein expression in GFAP transgenic flies. $N = 3$. ** $p < 0.01$. **c**, Genetic inhibition of glial caspase activity markedly increases p53 protein expression in GFAP transgenic flies. $N = 8$. ** $p < 0.01$. **d**, Genetic inhibition of glial caspase activity markedly increases pH2Av protein expression in GFAP transgenic flies. $N = 6$. * $p < 0.05$. **e**, Genetic inhibition of glial caspase activity markedly increases the percentage of glial cells with senescence-associated HP1 α heterochromatin foci (SAHF) in GFAP transgenic flies. $N = 6$ per genotype. Blots were reprobed with an antibody to actin to illustrate equivalent protein loading. ** $p < 0.01$. One-way ANOVA with multiple comparison was used for statistical analysis. Flies are 20 d old.

senescence in our transgenic fly brains. The levels of the matrix metalloproteinase Mmp1, the single secreted MMP family member present in *Drosophila* (Stevens and Page-McCaw, 2012), were significantly increased by Western blot analysis (Fig. 2d). Similarly, there were significantly increased numbers of HP1 α -positive nuclear foci in glia (Fig. 2e, arrows), consistent with the presence of senescence associated heterochromatic foci. With the development of senescence HP1, redistributes from a more diffuse nuclear staining pattern to nuclear foci enriched in repressive epigenetic marks (Hernandez-Segura et al., 2018). We have previously demonstrated that p53 and pH2Av are induced in Alexander disease glial cells (Wang et al., 2015). We now demonstrate that these markers are specifically

expressed in glial cells with upregulation of the *upd* cytokine (Fig. 2f,g, arrows).

We next investigated the relationship of caspase activation and *upd* cytokine activation by co-labeling brain sections from GFAP transgenic flies with the *upd3-lacZ* reporter and the transgenic caspase reporter. Unexpectedly, we found that glia with caspase activation (Fig. 3a, arrows) did not upregulate *upd3* (Fig. 3a, arrowhead). Further, cells expressing *upd3* (Fig. 3b, arrowhead) were not TUNEL-positive (Fig. 3b, arrow) either, consistent with a distinction between the two populations of abnormal glial cells.

Given the striking neurotoxicity observed following caspase inhibition (Fig. 1), but dissociation between glial cytokine

activation and current caspase activation (Fig. 3a), we wondered whether the toxic glial secretory phenotype might reflect prior caspase activation. To mark cells with past caspase activation, or anastasis, we used the transgenic CasExpress reporter (Ding et al., 2016). In the CasExpress reporter system the GAL4 transcription factor is maintained in an inactive state by tethering to the plasma membrane. Upon caspase activation and cleavage of the tether GAL4 can enter the nucleus and activate gene transcription. The G-trace reporter system (Evans et al., 2009) is then used to monitor prior cleavage of the reporter via GFP expression. When we introduced the CasExpress reporter system into our GFAP transgenic fly model we found that significant numbers of glial cells demonstrated evidence of prior caspase activation, as indicated by GFP expression as monitored by immunostaining (Fig. 3c, arrows, d) or Western blot analysis (Fig. 3e). Importantly, and in contrast to cells with current caspase activation (Fig. 3a), cells with prior caspase activation also showed *upd3-lacZ* upregulation (Fig. 3c, arrows). As described previously (Ding et al., 2016), some glia in control flies not expressing human GFAP also showed evidence of prior caspase activation (Fig. 3c, arrowheads, d,e). The majority of cells with GFAP-associated prior caspase activation appeared to up regulate *upd3-lacZ*, although the precise relationship between caspase activation and *upd3* expression will require longitudinal assessment of the same glial cells over time.

To test our hypothesis that caspase activation drives neurotoxicity by promoting glial senescence we examined expression of the cytokine reporter *upd3-lacZ* following genetic caspase inhibition. We observed significantly increased reporter expression with expression of the antiapoptotic protein p35 or removal of one copy of *reaper*, *hid*, and *grim* with the H99 deficiency (Fig. 4a). Similarly, reducing caspase activation in glia also increased Mmp1 levels (Fig. 4b), p53 (Fig. 4c), and pH2Av (Fig. 4d) and the number of HP1 α -positive nuclear foci (Fig. 4e). Expression of *upd3-lacZ*, activation of the CasExpress reporter or expression of senescence-associated markers was not confined to a particular population of glial cells as indicated by cell morphology or localization, but further work using reagents to identify specific glial populations would be required to investigate the possibility of subtype vulnerability in more detail.

The *upd* cytokines, including *upd3*, signal through the transmembrane receptor *dome*, which shares sequence and functional homology with the mammalian IL-6 receptor family (Vanha-Aho et al., 2016). We inhibited expression of the *dome* receptor using a heterozygous loss of function mutation (*dome*^{G0441}) or transgenic RNAi to determine the functional consequences of increased *upd3* expression. When we reduced *dome* expression in glia we significantly reduced total cell death (Fig. 5a,b) and

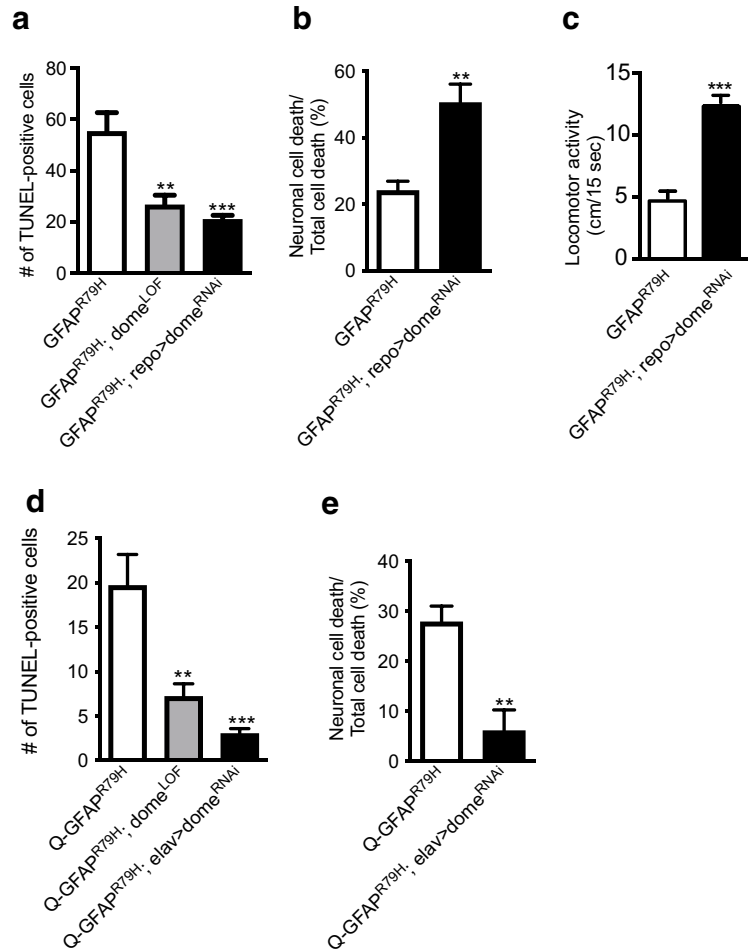


Figure 5. Genetic inhibition of *dome* rescues GFAP toxicity in Alexander disease model flies. **a**, Genetic inhibition of *dome* in glial cells reduces the number of TUNEL-positive cells in GFAP transgenic flies. $N \geq 6$ per genotype. ** $p < 0.01$, *** $p < 0.001$. **b**, Genetic inhibition of *dome* in glial cells increases the percentage of neuronal cell death. $N = 6$ per genotype. ** $p = 0.0020$. **c**, Genetic inhibition of *dome* in glial cells increases locomotor activity in Alexander disease model flies. $N \geq 11$ per genotype. *** $p < 0.0001$. **d**, Genetic inhibition of *dome* in neurons using the pan-neuronal driver *elav-GAL4* reduces the number of TUNEL-positive cells in flies expressing GFAP in glia using the pan-glial driver *repo-QF2*. $N \geq 6$ per genotype. ** $p < 0.01$, *** $p < 0.001$. **e**, Genetic inhibition of *dome* in neurons reduces the percentage of neuronal cell death in flies expressing GFAP in glia. $N \geq 6$ per genotype. ** $p = 0.0015$. One-way ANOVA with multiple comparison analysis was used in **a**, **d** and unpaired *t* test was used in **b**, **c**, **e** for statistical analysis. Flies are 20 d old in **a–c** and 30 d old in **d**, **e**.

locomotor dysfunction (Fig. 5c), consistent with an autocrine function for *upd3*. The proportion of glial cell death decreased (Fig. 5b), consistent with an effect of the *dome* receptor in glia when *repo-GAL4* driven *dome* RNAi was used. Given the striking increase in neurodegeneration with inhibition of glial apoptosis (Fig. 1), we wondered whether the *upd3* cytokine might signal directly to neurons to promote neurotoxicity. We therefore employed a dual bipartite expression system in which human mutant GFAP^{R79H} is controlled using the QF2 system (Riabinina et al., 2015) and the pan-glial *repo-QF2* driver, and the GAL4 system is employed to regulate gene expression in neurons (Wang et al., 2015). Blocking the *dome* cytokine in neurons while expressing mutant GFAP in glia significantly reduced the total number of apoptotic cells (Fig. 5d), and markedly decreased neuronal death (Fig. 5e), without changing GFAP levels (Extended Data Fig. 1–1g).

We next determined whether glial cells in a vertebrate animal model of Alexander disease exhibited markers of senescence. We used a recently described rat model in which the GFAP^{R237H}

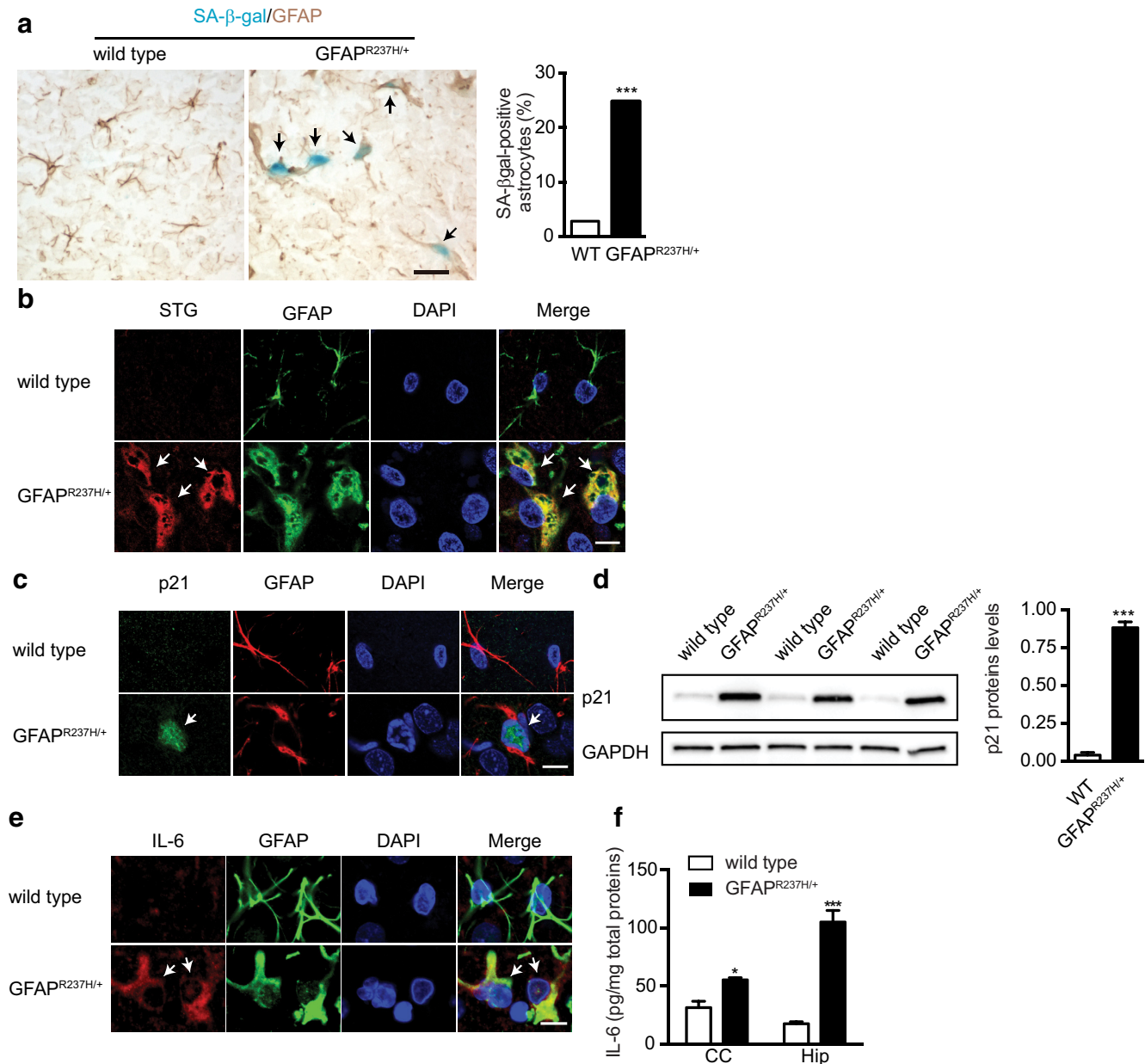


Figure 6. Astrocytes in the rat model of Alexander disease exhibit senescent phenotypes. **a**, Bright field images show SA-β-gal staining (blue) in the astrocytes (brown staining) of cortex from eight-week-old Alexander disease model rats, but not in age-matched wild-type rats. Tissue was also stained with GFAP to mark astrocytes (brown). Scale bar: 50 μm. Quantification is in the right panel. *** $p < 0.0001$, χ^2 test. $N > 350$ astrocytes per genotype was used for quantification. **b**, Double label immunofluorescence shows senescent astrocytes labeled by SenTraGor (STG) compound in eight-week-old Alexander disease model rats (arrows, bottom panel), but not in age-matched wild-type rats. GFAP marks astrocytes. DAPI labels nuclei. Scale bar: 10 μm. **c**, Double label immunofluorescence shows activation of p21^{clp/waf1} in the astrocytes of eight-week-old Alexander disease model rats (arrow, bottom panel), but not in age-matched wild-type rats. GFAP marks astrocytes. DAPI labels nuclei. Scale bar: 10 μm. **d**, Western blotting demonstrates marked increase of p21^{clp/waf1} expression in the hippocampus of eight-week-old Alexander disease model rats compared with age-matched wild-type rats. The blot was reprobed with an antibody to GAPDH to illustrate equivalent protein loading. *** $p < 0.0001$, unpaired t test. **e**, Double label immunofluorescence shows IL-6 expression in the astrocytes of eight-week-old Alexander disease model rats (arrow, bottom panel), but not in age-matched wild-type rats. GFAP marks astrocytes. DAPI labels nuclei. Scale bar: 10 μm. **f**, Immunoassay demonstrates marked increases of IL-6 concentration in eight-week-old Alexander disease model rats compared with age-matched wild-type rats. $N = 3$ per genotype per region. CC: corpus callosum; Hip: hippocampus. * $p < 0.05$, *** $p < 0.0001$, multiple t tests.

mutation, orthologous with the severe GFAP^{R239H} human mutation, has been introduced by CRISPR/Cas9 targeting of the rat GFAP gene (Hagemann et al., 2021). We began by assessing senescence-associated β-galactosidase activity, a canonical hallmark of senescence in vertebrate systems that reflects the increased lysosomal content present during senescence (Dimri et al., 1995; Hernandez-Segura et al., 2018). When cryosections from Alexander model rats were compared with wild-type littermates a significant increase in β-galactosidase staining was

observed (Fig. 6a). Double label histochemistry revealed that β-galactosidase-positive cells were astrocytes (Fig. 6a, arrows). We next monitored the accumulation of the aging-related pigment lipofuscin using the sensitive and specific biotin-linked Sudan black B derivative SenTraGor (Evangelou et al., 2017). Astrocytes from Alexander disease model rats exhibited frequent lipofuscin accumulation (Fig. 6b, arrows), while no lipofuscin could be detected in control rats at the eight-week time point examined.

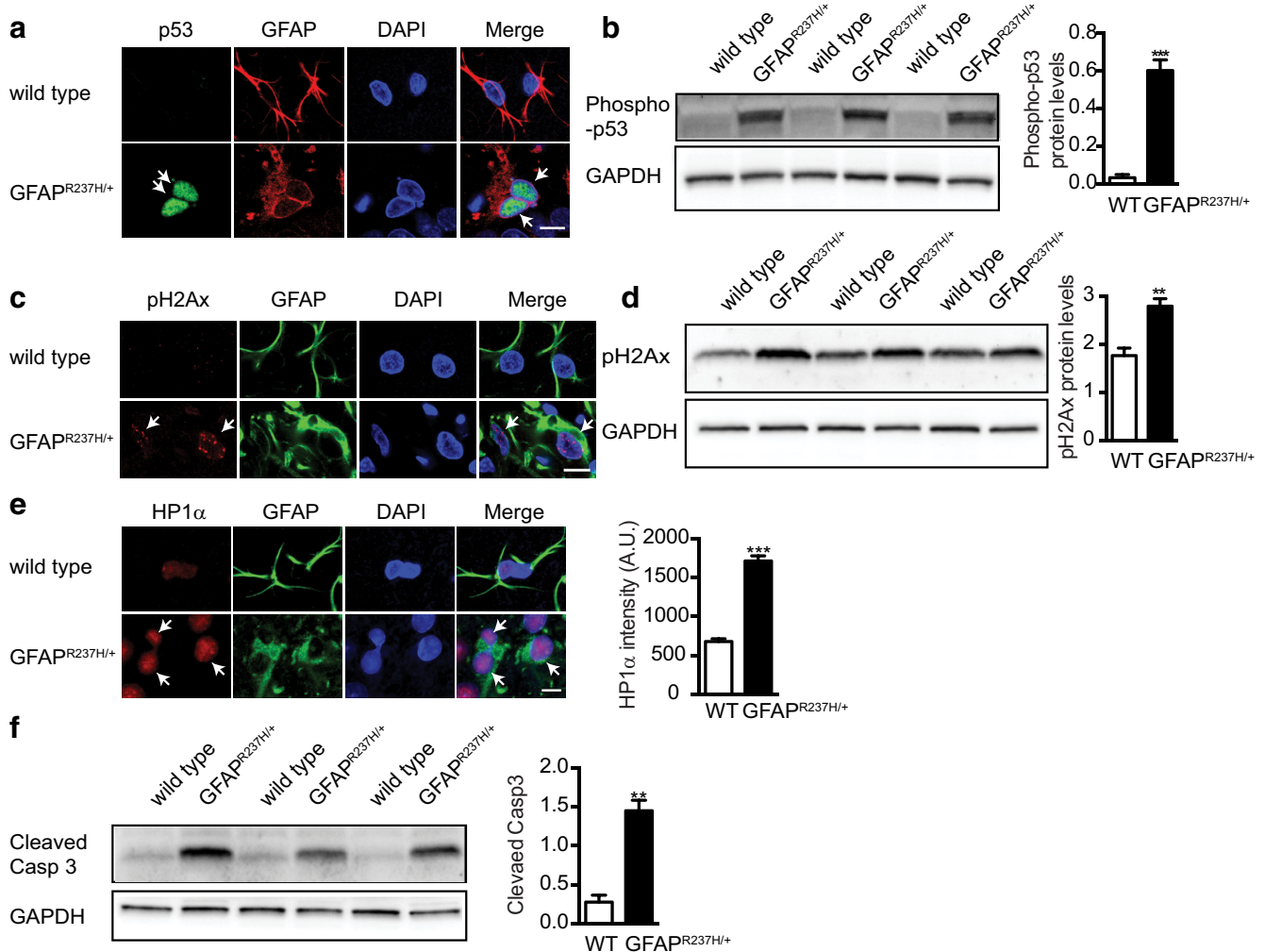


Figure 7. DNA damage response is activated in the astrocytes of Alexander disease model rats. **a**, Double label immunofluorescence shows activation of p53 in the astrocytes of eight-week-old Alexander disease model rats (arrows, bottom panel), but not in age-matched wild-type rats. GFAP marks astrocytes. DAPI labels nuclei. Scale bar: 10 μ m. **b**, Western blotting demonstrates increased expression of phospho-p53 (Ser15) in the hippocampus of eight-week-old Alexander disease model rats (GFAP^{R237H/+}) compared with age-matched wild-type rats. GAPDH was used as a loading control. $N = 3$ per genotype. $***p = 0.0007$, unpaired t test. **c**, Double label immunofluorescence shows activation of DNA damage marker pH2Ax in the astrocytes of eight-week-old Alexander disease model rats (arrows, bottom panel), but not in age-matched wild-type rats. GFAP marks astrocytes. DAPI labels nuclei. Scale bar: 10 μ m. **d**, Western blotting demonstrates increased expression of phospho-H2Ax (pH2Ax) in the hippocampus of eight-week-old Alexander disease model rats (GFAP^{R237H/+}) compared with age-matched wild-type rats. GAPDH was used as a loading control. $N = 3$ per genotype. $**p = 0.0098$, unpaired t test. **e**, Double label immunofluorescence and quantification show increased expression of HP1 α in the astrocytes of Alexander disease model rats than in wild-type animals. GFAP marks astrocytes. DAPI labels nuclei. Scale bar: 5 μ m. HP1 α intensity was quantified using ImageJ. $N = 3$ rats per genotype. At least 20 astrocytes were imaged and quantified from each animal. $***p < 0.0001$, unpaired t test. **f**, Western blotting demonstrates increased expression of cleaved caspase-3 in the hippocampus of eight-week-old Alexander disease model rats (GFAP^{R237H/+}) compared with age-matched wild-type rats. The blot was reprobed with an antibody to GAPDH to illustrate equivalent protein loading. $N = 3$ per genotype. $**p = 0.0019$, unpaired t test.

The cell cycle inhibitory protein p21 plays an important role in inducing cellular senescence and is frequently used to identify senescent cells (Takeuchi et al., 2010; Demaria et al., 2014). Astrocytes in Alexander disease model rats displayed nuclear accumulation of p21 as assessed by immunofluorescence (Fig. 6c, arrows) and Western blotting (Fig. 6d). To determine whether senescent astrocytes upregulated cytokine expression, as observed in Alexander disease model flies (Figs. 2–4), we examined IL-6 levels by immunostaining and immunoassay and found that the rat model astrocytes expressed increased IL-6 compared with littermate controls (Fig. 6e, arrows, f). We focused on IL-6 because the upd family cytokines signal through the dome receptor, which shares sequence and functional homology with the IL-6 receptor family (Vanha-Aho et al., 2016). Further, IL-6 signals through activation of the JAK/STAT pathway and we have demonstrated that phosphorylated STAT3 is

elevated in Alexander disease model rats and mice (LaPash Daniels et al., 2012; Hagemann et al., 2021).

The DNA damage response is a key hallmark of cellular senescence (Hernandez-Segura et al., 2018). We have previously demonstrated a robust DNA damage response, including p53 and pH2AX induction, in glia from fly and mouse models of Alexander disease (Wang et al., 2015). To determine whether Alexander disease model rats also show activation of the DNA damage response, we began by assessing p53. We found robust upregulation of p53 in glia from rats expressing mutant GFAP (Fig. 7a, arrows). Similarly, Western blotting revealed significantly increased levels of p53 phosphorylated at serine 15 (Fig. 7b). We additionally observed multiple nuclear foci positive for pH2Ax in mutant astrocytes (Fig. 7c) and increased pH2Ax by Western blotting (Fig. 7d), consistent with induction of DNA double-strand breaks. Consistent with findings from *Drosophila*,

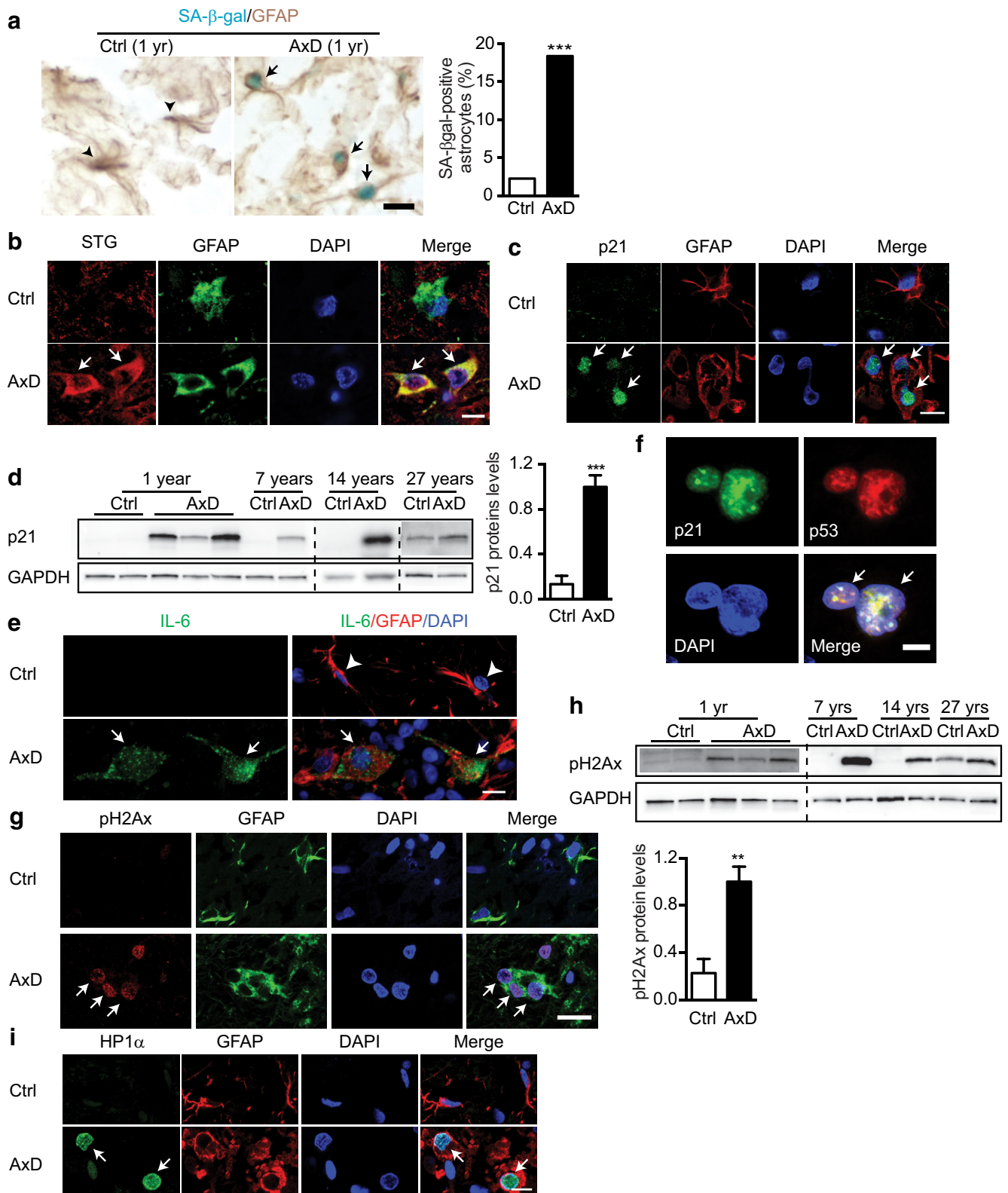


Figure 8. Astrocytes in Alexander disease patient tissue show senescent phenotypes. **a**, Bright field images show SA- β -gal staining (blue) in the astrocytes of a one-year-old Alexander disease patient tissue (arrows), but not in an age-matched control tissue (arrowheads). Tissue was also stained with GFAP to mark astrocytes (brown). Scale bar: 20 μ m. Quantification is in the right panel. ***p < 0.0001, χ^2 test. N > 500 astrocytes per genotype was used for quantification. **b**, Double label immunofluorescence shows senescent astrocytes labeled by SenTraGor (STG) compound in a one-year-old Alexander disease patient tissue (arrows), but not in an age-matched control tissue. GFAP marks astrocytes. DAPI labels nuclei. Scale bar: 5 μ m. **c**, Double label immunofluorescence shows activation of p21^{clp/waf1} in the astrocytes of a one-year-old Alexander disease patient tissue (arrows), but not in an age-matched control. GFAP marks astrocytes. DAPI labels nuclei. Scale bar: 10 μ m. **d**, Western blotting demonstrates a marked increase of p21^{clp/waf1} expression in Alexander disease patient tissue compared with age-matched controls. ***p = 0.0001, unpaired t test. **e**, Double label immunofluorescence shows IL-6 expression in the astrocytes of a one-year-old Alexander disease patient tissue (arrows), but not in an age-matched control. GFAP marks astrocytes. DAPI labels nuclei. Scale bar: 10 μ m. **f**, Double label immunofluorescence shows colocalization of p21^{clp/waf1} and p53 (arrows) in a one-year-old Alexander disease patient. Scale bar: 10 μ m. **g**, Double label immunofluorescence shows activation of phospho-H2Ax in the astrocytes of a one-year-old Alexander disease patient tissue

Alexander disease rat model astrocytes also showed increased staining for HP1 α (Fig. 7e) and elevated levels of activated caspase-3 (Fig. 7f). Expression of senescence-associated β -galactosidase, other senescence-related markers, and DNA damage markers were widespread in Alexander disease model rats, involving both gray and white matter without obviously sparing specific anatomic areas, but further work will be required to define the subtype(s) of astrocytes affected in more detail.

We then explored the relevance of our animal model work to the human disease by examining markers of senescence in post-mortem brain tissue from patients with Alexander disease and control individuals. Staining of cryosections of the available frontal cortical brain tissue from patients revealed increased senescence-associated β -galactosidase activity in astrocytes (Fig. 8a). Similarly, astrocytes from patients accumulated increased aging-related lipofuscin pigment labeled with SenTraGor (Fig. 8b, arrows) and nuclear p21 (Fig. 8c, arrows, d). Patient astrocytes also displayed increased levels of IL-6 (Fig. 8e). p21-positive patient astrocytes also showed p53 upregulation (Fig. 8f). As in the fly, rat and mouse models, patient astrocytes showed evidence of DNA double-strand breaks, with accumulation of pH2Ax seen by immunofluorescence (Fig. 8g, arrows) and quantitative Western blotting (Fig. 8h). Similarly, HP1 α was increased in astrocyte nuclei in patient brain tissue (Fig. 8i).

We have recently generated iPSCs from Alexander disease patients and demonstrated that they replicate key cellular features of the disorder (Jones et al., 2018; Wang et al., 2018). We examined markers of cellular senescence in patient-derived astrocytes in culture and observed significantly increased senescence-associated β -galactosidase activity (Fig. 9a). Other markers of senescence, including p21, p53, pH2Ax, and IL-6 were also increased in patient-derived astrocytes (Fig. 9).

Discussion

Anastasis is the process of cellular recovery following activation of apoptosis (Tang et al., 2012; Tang and Tang, 2018) or ferroptosis (Tang and Tang, 2019). The process has been best defined in cell culture systems where a cell death signal, such as ethanol (Tang et al., 2012), is provided and the apoptotic cascade is triggered. The cell death inducer is then washed away and the cells allowed to recover. In these *in vitro* experiments, cells can recover viability even after markers of late-stage cell death, including executioner caspase activation, nuclear condensation, membrane blebbing and cell shrinkage, have occurred.

Although anastasis has been observed by multiple groups in cell culture (Sun et al., 2017; Tang et al., 2017; Seervi et al., 2019), results *in vitro* do not address the *in vivo* role of anastasis. Therefore systems to identify and study anastasis in animals have been developed. Here, we have used the transgenic CasExpress reporter (Ding et al., 2016) to study anastasis in a *Drosophila* model of the astroglialopathy Alexander disease (Wang et al., 2011). The CasExpress reporter is based on the caspase-3-dependent cleavage of a membrane tethered transcription factor, subsequent translocation to the nucleus and irreversible

induction of reporter gene expression through excision of a transcriptional stop cassette. Using the CasExpress system Ding et al. (2016) demonstrated widespread survival of cells with a history of caspase-3 activation in *Drosophila*. Comparable results were obtained by a second group using a similar reporter, termed CaspaseTracker (Tang et al., 2015).

Since non-apoptotic roles of caspase activation have been clearly documented (Nakajima and Kuranaga, 2017), and cells *in vivo* cannot be studied in the same longitudinal detail possible *in vitro*, differentiation of anastasis from “caspase-dependent non-lethal cellular processes” (Aram et al., 2017) may be challenging (Sun and Montell, 2017). Using the CaspaseTracker reporter Tang et al. (2015) found that exposure of *Drosophila* to transient environmental stress induced reporter expression in egg chambers with activated caspase immunoreactivity, apoptotic morphologies and a known genetic role for activated caspase in promoting stress-induced cell death, strongly arguing that CaspaseTracker identified cells that had undergone anastasis. Similarly, we find that expression of toxic mutant GFAP^{R79H} activates the CasExpress reporter in fly glia (Fig. 3). We have also shown that glia have activated caspase immunoreactivity (Fig. 3a) and undergo TUNEL-positive cell death (Wang et al., 2011, 2015). We therefore interpret glial cells labeled with the CasExpress reporter in our GFAP^{R79H} transgenic flies to have recovered from apoptosis.

Mechanisms controlling anastasis are beginning to emerge. Gene expression and proteomic profiling of cultured cells undergoing anastasis are consistent with multiple phases of the process and have suggested candidate pathways controlling recovery from death (Sun et al., 2017; Tang et al., 2017; Seervi et al., 2019). Of note, regulation of oxidative stress and the actin cytoskeleton has emerged from profiling studies (Sun et al., 2017; Seervi et al., 2019). These findings are intriguing because we have previously implicated oxidative stress (Hagemann et al., 2005; Wang et al., 2011) and control of actin cytoskeletal dynamics (Wang et al., 2018) in the pathogenesis of Alexander disease. The substantial genetic resources available in *Drosophila* may facilitate future mechanistic studies of pathways controlling anastasis in our model. A better mechanistic understanding of the processes controlling the onset and maintenance of anastasis will be important for development of rational treatment strategies aimed at modulating cell death pathways.

While anastasis might have evolved as a method to preserve cell viability following a severe, but transient stress (Sun and Montell, 2017; Sun et al., 2017), in our system rescuing glia from apoptosis promotes behavioral deficits and neurodegeneration (Fig. 1). Anastasis may also be maladaptive in the context of malignancy. Tumor cells exposed to transient chemotherapy or radiotherapy may use anastasis to escape from antineoplastic therapy. Additionally, tumor cells that have undergone anastasis may be more migratory (Sun et al., 2017) and genetically unstable (Ichim et al., 2015), further promoting spread of tumor cells and evolution to higher grade lesions.

In our system, we implicate the premature development of senescence in glia as the mechanism by which anastasis promotes disease pathogenesis. A compelling body of literature has related the development of cellular senescence with disease and aging (Gorgoulis et al., 2019), including in the brain (Baker and Petersen, 2018). Importantly, clearing senescent cells can improve cognitive function in mouse models of neurodegeneration (Bussian et al., 2018; Zhang et al., 2019) and decrease aging-related brain pathology (Yousefzadeh et al., 2018). Although increased senescence of both neurons and glia have been reported

(arrows) compared with age-matched control tissue. Scale bar: 10 μ m. **h**, Western blotting demonstrates increased phospho-H2Ax expression in Alexander disease patient tissue compared with age-matched controls. ****** p = 0.0019, unpaired t test. Blots were reprobed with an antibody to GAPDH to illustrate equivalent protein loading. **i**, Double label immunofluorescence shows increased HP1 α expression in the astrocytes of Alexander disease patient tissue (arrows) compared with age-matched control tissue. Scale bar: 10 μ m.

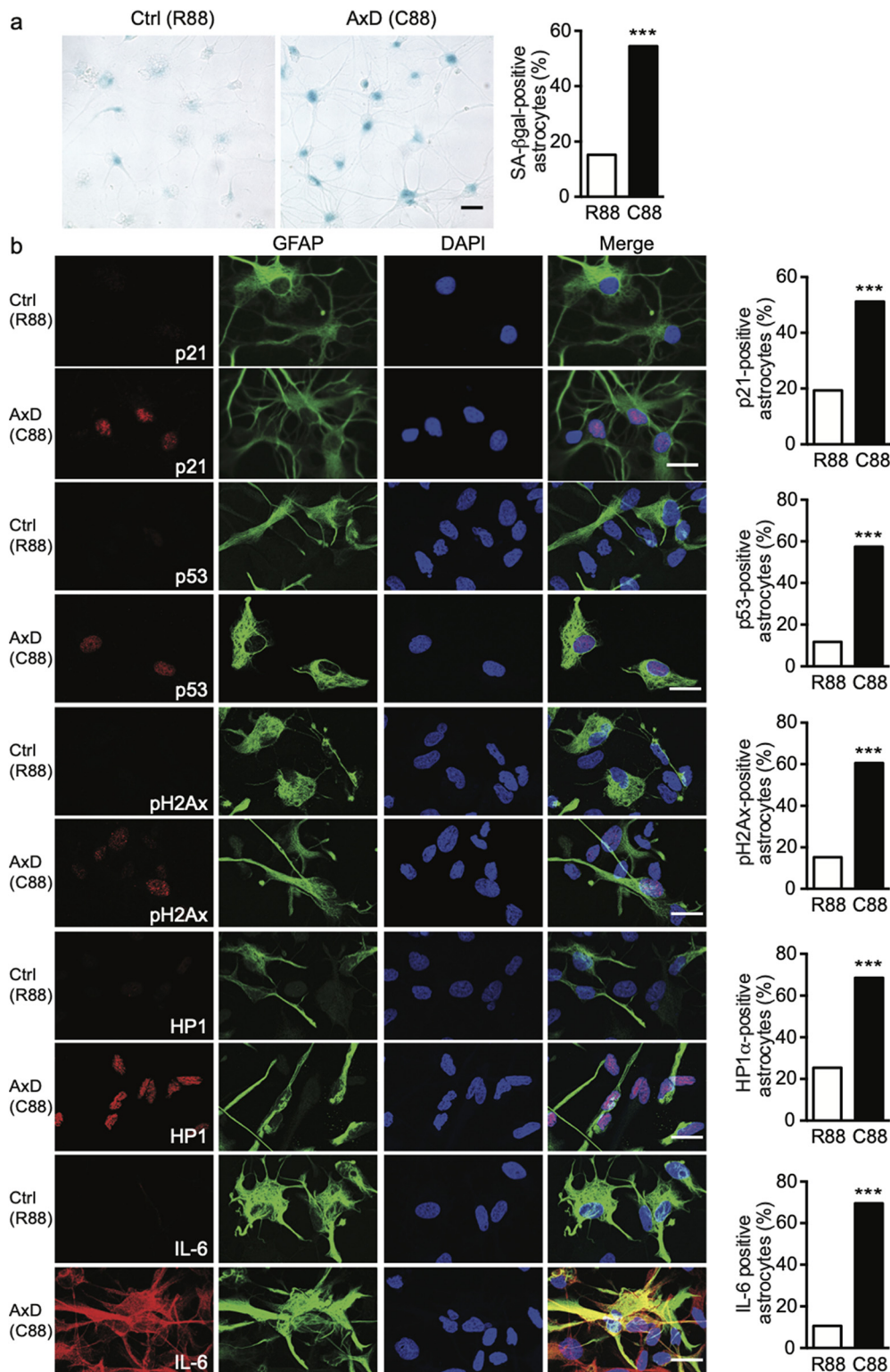


Figure 9. Alexander disease astrocytes recapitulate key *in vivo* senescent phenotypes. **a**, Bright field images of Alexander disease astrocytes (C88) and corrected control cells (R88) stained with SA-β-gal staining. Quantification shows a marked increase of the percentage of SA-β-gal-positive cells in Alexander disease astrocytes (C88) compared with corrected control astrocytes (R88). Scale bar: 25 μm. SA-β-gal staining intensity was quantified using ImageJ and the threshold was set at 170 for positive cells. $N = 1061$ (C88) and 1300 (R88). $***p < 0.0001$, χ^2 test. **b**, Double label immunofluorescence and quantification confirm increased activation of p21^{clp/waf1}, p53, pH2Ax, HP1 α , and IL-6 in Alexander disease astrocytes (C88) compared with corrected control cells (R88). GFAP marks astrocytes. DAPI labels nuclei. Scale bar: 20 μm. $N > 200$ cells per genotype in each quantification. $***p < 0.0001$, χ^2 test.

in neurologic disease and in model of the disorders (Bussian et al., 2018; Chinta et al., 2018; Riessland et al., 2019), we observe markers of senescence restricted to astrocytes in Alexander disease patients and in experimental models of the disorder.

Here, we have taken a multifaceted experimental approach integrating genetics and cell biology in *Drosophila*, rat and humans to provide strong evidence for toxic anastasis mediated by astrocyte senescence, which drives non-cell autonomous

neurodegeneration, in the primary astroglialopathy Alexander disease. Targeting the anastasis-driven astrocyte senescence we outline here may provide new opportunities for therapy in Alexander disease, a severe and currently untreatable disorder. In addition, given the increasing evidence for glial dysfunction and well-known GFAP upregulation in many neurologic disorders, modulation of toxic anastasis and senescence may be a therapeutic target in other diseases of the central nervous system as well.

References

- Aram L, Yacobi-Sharon K, Arama E (2017) CDPs: caspase-dependent non-lethal cellular processes. *Cell Death Differ* 24:1307–1310.
- Baker DJ, Petersen RC (2018) Cellular senescence in brain aging and neurodegenerative diseases: evidence and perspectives. *J Clin Invest* 128:1208–1216.
- Brenner M, Goldman JE, Quinlan RA, Messing A (2009) Alexander disease: a genetic disorder of astrocytes. In: *Astrocytes in (patho)physiology of the nervous system*, pp 591–648. New York: Springer.
- Bussian TJ, Aziz A, Meyer CF, Swenson BL, van Deursen JM, Baker DJ (2018) Clearance of senescent glial cells prevents tau-dependent pathology and cognitive decline. *Nature* 562:578–582.
- Chen P, Nordstrom W, Gish B, Abrams JM (1996) grim, a novel cell death gene in *Drosophila*. *Genes Dev* 10:1773–1782.
- Chinta SJ, Woods G, Demaria M, Rane A, Zou Y, McQuade A, Rajagopalan S, Limbad C, Madden DT, Campisi J, Andersen JK (2018) Cellular senescence is induced by the environmental neurotoxin paraquat and contributes to neuropathology linked to Parkinson's disease. *Cell Rep* 22:930–940.
- Demaria M, Ohtani N, Youssef SA, Rodier F, Toussaint W, Mitchell JR, Laberge RM, Vijg J, Van Steeg H, Dollé MET, Hoeijmakers JHJ, de Bruin A, Hara E, Campisi J (2014) An essential role for senescent cells in optimal wound healing through secretion of PDGF-AA. *Dev Cell* 31:722–733.
- Dimri GP, Lee X, Basile G, Acosta M, Scott G, Roskelley C, Medrano EE, Linskens M, Rubelj I, Pereira-Smith O (1995) A biomarker that identifies senescent human cells in culture and in aging skin in vivo. *Proc Natl Acad Sci USA* 92:9363–9367.
- Ding AX, Sun G, Argaw YG, Wong JO, Easwaran S, Montell DJ (2016) CasExpress reveals widespread and diverse patterns of cell survival of caspase-3 activation during development in vivo. *Elife* 5:e10936.
- Evangelou K, Lougiakis N, Rizou SV, Kotsinas A, Kletsas D, Muñoz-Espín D, Kastrinakis NG, Pouli N, Marakos P, Townsend P, Serrano M, Bartek J, Gorgoulis VG (2017) Robust, universal biomarker assay to detect senescent cells in biological specimens. *Aging Cell* 16:192–197.
- Evans CJ, Olson JM, Ngo KT, Kim E, Lee NE, Kuoy E, Patananan AN, Sitz D, Tran P, Do M-T, Yackel K, Cespedes A, Hartenstein V, Call GB, Banerjee U (2009) G-TRACE: rapid Gal4-based cell lineage analysis in *Drosophila*. *Nat Methods* 6:603–605.
- Goldman JE, Corbin E (1988) Isolation of a major protein component of Rosenthal fibers. *Am J Pathol* 130:569–578.
- Gorgoulis V, Adams PD, Alimonti A, Bennett DC, Bischof O, Bishop C, Campisi J, Collado M, Evangelou K, Ferbeyre G, Gil J, Hara E, Krizhanovsky V, Jurk D, Maier AB, Narita M, Niedernhofer L, Passos JF, Robbins PD, Schmitt CA, et al. (2019) Cellular senescence: defining a path forward. *Cell* 179:813–827.
- Hagemann TL, Gaeta SA, Smith MA, Johnson DA, Johnson JA, Messing A (2005) Gene expression analysis in mice with elevated glial fibrillary acidic protein and Rosenthal fibers reveals a stress response followed by glial activation and neuronal dysfunction. *Hum Mol Genet* 14:2443–2458.
- Hagemann TL, Connor JX, Messing A (2006) Alexander disease-associated glial fibrillary acidic protein mutations in mice induce Rosenthal fiber formation and a white matter stress response. *J Neurosci* 26:11162–11173.
- Hagemann TL, Boelens WC, Wawrousek EF, Messing A (2009) Suppression of GFAP toxicity by α B-crystallin in mouse models of Alexander disease. *Hum Mol Genet* 18:1190–1199.
- Hagemann TL, Jobe EM, Messing A (2012) Genetic ablation of Nrf2/antioxidant response pathway in Alexander disease mice reduces hippocampal gliosis but does not impact survival. *PLoS One* 7:e37304.
- Hagemann TL, Powers B, Lin NH, Mohamed A, Dague KL, Hannah SC, Bachman G, Mazur C, Rigo F, Olsen AL, Feany MB, Perng MD, Berman RF, Messing A (2021) Antisense therapy in a rat model of Alexander disease reverses GFAP pathology, white matter deficits, and motor impairment. *Sci Transl Med* 13:eabg4711.
- Hartl FU (2017) Protein misfolding diseases. *Annu Rev Biochem* 86:21–26.
- Hay BA, Wolff T, Rubin GM (1994) Expression of baculovirus P35 prevents cell death in *Drosophila*. *Development* 120:2121–2129.
- Heaven MR, Flint D, Randall SM, Sosunov AA, Wilson L, Barnes S, Goldman JE, Muddiman DC, Brenner M (2016) Composition of Rosenthal fibers, the protein aggregate hallmark of Alexander disease. *J Proteome Res* 15:2265–2282.
- Hernandez-Segura A, Nehme J, Demaria M (2018) Hallmarks of cellular senescence. *Trends Cell Biol* 28:436–453.
- Ichim G, Lopez J, Ahmed SU, Muthalagu N, Giampazolias E, Delgado ME, Haller M, Riley JS, Mason SM, Athineos D, Parsons MJ, van de Kooij B, Bouchier-Hayes L, Chalmers AJ, Rooswinkel RW, Oberst A, Blyth K, Rehm M, Murphy DJ, Tait SWG (2015) Limited mitochondrial permeabilization causes DNA damage and genomic instability in the absence of cell death. *Mol Cell* 57:860–872.
- Johnson AB, Bettica A (1989) On-grid immunogold labeling of glial intermediate filaments in epoxy-embedded tissue. *Am J Anat* 185:335–341.
- Jones JR, Kong L, Hanna MG, Hoffman B, Krencik R, Bradley R, Hagemann T, Choi J, Doers M, Dubovis M, Sherfat MA, Bhattacharyya A, Kendziorci K, Audhya A, Messing A, Zhang SC (2018) Mutations in GFAP disrupt the distribution and function of organelles in human astrocytes. *Cell Rep* 25:947–958.e4.
- Koyama Y, Goldman JE (1999) Formation of GFAP cytoplasmic inclusions in astrocytes and their disaggregation by α B-crystallin. *Am J Pathol* 154:1563–1572.
- LaPash Daniels CM, Austin EV, Rockney DE, Jacka EM, Hagemann TL, Johnson DA, Johnson JA, Messing A (2012) Beneficial effects of Nrf2 overexpression in a mouse model of Alexander disease. *J Neurosci* 32:10507–10515.
- Martín FA, Pérez-Garijo A, Morata G (2009) Apoptosis in *Drosophila*: compensatory proliferation and undead cells. *Int J Dev Biol* 53:1341–1347.
- Messing A, Brenner M, Feany MB, Nedergaard M, Goldman JE (2012) Alexander disease. *J Neurosci* 32:5017–5023.
- Nakajima YI, Kuranaga E (2017) Caspase-dependent non-apoptotic processes in development. *Cell Death Differ* 24:1422–1430.
- Neves J, Demaria M, Campisi J, Jasper H (2015) Of flies, mice, and men: evolutionarily conserved tissue damage responses and aging. *Dev Cell* 32:9–18.
- Pérez-Garijo A, Martín FA, Morata G (2004) Caspase inhibition during apoptosis causes abnormal signalling and developmental aberrations in *Drosophila*. *Development* 131:5591–5598.
- Riabinina O, Luginbuhl D, Marr E, Liu S, Wu MN, Luo L, Potter CJ (2015) Improved and expanded Q-system reagents for genetic manipulations. *Nat Methods* 12:219–222, 5 p following 222.
- Riessland M, Kolisnyk B, Kim TW, Cheng J, Ni J, Pearson JA, Park EJ, Dam K, Acehan D, Ramos-Espíritu LS, Wang W, Zhang J, Shim JW, Cicci G, Brichta L, Studer L, Greengard P (2019) Loss of SATB1 induces p21-dependent cellular senescence in post-mitotic dopaminergic neurons. *Cell Stem Cell* 25:514–530.e8.
- Seervi M, Sumi S, Chandrasekharan A, Sharma AK, SanthoshKumar TR (2019) Molecular profiling of anastatic cancer cells: potential role of the nuclear export pathway. *Cell Oncol (Dordr)* 42:645–661.
- Stevens LJ, Page-McCaw A (2012) A secreted MMP is required for reepithelialization during wound healing. *Mol Biol Cell* 23:1068–1079.
- Sun G, Montell DJ (2017) Q&A: cellular near death experiences-what is anastasis? *BMC Biol* 15:92.
- Sun G, Guzman E, Balasanyan V, Conner CM, Wong K, Zhou HR, Kosik KS, Montell DJ (2017) A molecular signature for anastasis, recovery from the brink of apoptotic cell death. *J Cell Biol* 216:3355–3368.
- Takeuchi S, Takahashi A, Motoi N, Yoshimoto S, Tajima T, Yamakoshi K, Hirao A, Yanagi S, Fukami K, Ishikawa Y, Sone S, Hara E, Ohtani N (2010) Intrinsic cooperation between p16INK4a and p21Waf1/Cip1 in the onset of cellular senescence and tumor suppression in vivo. *Cancer Res* 70:9381–9390.

- Tang HL, Tang HM, Mak KH, Hu S, Wang SS, Wong KM, Wong CST, Wu HY, Law HT, Liu K, Talbot CC, Lau WK, Montell DJ, Fung MC (2012) Cell survival, DNA damage, and oncogenic transformation after a transient and reversible apoptotic response. *Mol Biol Cell* 23:2240–2252.
- Tang HL, Tang HM, Fung MC, Hardwick JM (2015) In vivo CaspaseTracker biosensor system for detecting anastasis and non-apoptotic caspase activity. *Sci Rep* 5:9015.
- Tang HM, Tang HL (2018) Anastasis: recovery from the brink of cell death. *R Soc Open Sci* 5:180442.
- Tang HM, Tang HL (2019) Cell recovery by reversal of ferroptosis. *Biol Open* 8:bio043182.
- Tang HM, Talbot CC, Fung MC, Tang HL (2017) Molecular signature of anastasis for reversal of apoptosis. *Fl000Res* 6:43.
- Vanha-Aho L-M, Valanne S, Rämetsä M (2016) Cytokines in *Drosophila* immunity. *Immunol Lett* 170:42–51.
- Wang L, Colodner KJ, Feany MB (2011) Protein misfolding and oxidative stress promote glial-mediated neurodegeneration in an Alexander disease model. *J Neurosci* 31:2868–2877.
- Wang L, Hagemann TL, Kalwa H, Michel T, Messing A, Feany MB (2015) Nitric oxide mediates glial-induced neurodegeneration in Alexander disease. *Nat Commun* 6:8966.
- Wang L, Hagemann TL, Messing A, Feany MB (2016) An in vivo pharmacological screen identifies cholinergic signaling as a therapeutic target in glial-based nervous system disease. *J Neurosci* 36:1445–1455.
- Wang L, Xia J, Li J, Hagemann TL, Jones JR, Fraenkel E, Weitz DA, Zhang SC, Messing A, Feany MB (2018) Tissue and cellular rigidity and mechanosensitive signaling activation in Alexander disease. *Nat Commun* 9:1899.
- Williams DW, Kondo S, Krzyzanowska A, Hiromi Y, Truman JW (2006) Local caspase activity directs engulfment of dendrites during pruning. *Nat Neurosci* 9:1234–1236.
- Yousefzadeh MJ, Zhu Y, McGowan SJ, Angelini L, Fuhrmann-Stroissnigg H, Xu M, Ling YY, Melos KI, Pirtskhalava T, Inman CL, McGuckian C, Wade EA, Kato JI, Grassi D, Wentworth M, Burd CE, Arriaga EA, Ladiges WL, Tchkonja T, Kirkland JL, et al. (2018) Fisetin is a senotherapeutic that extends health and lifespan. *EBioMedicine* 36:18–28.
- Zhang P, Kishimoto Y, Grammatikakis I, Gottimukkala K, Cutler RG, Zhang S, Abdelmohsen K, Bohr VA, Misra Sen J, Gorospe M, Mattson MP (2019) Senolytic therapy alleviates A β -associated oligodendrocyte progenitor cell senescence and cognitive deficits in an Alzheimer's disease model. *Nat Neurosci* 22:719–728.
- Zhou F, Rasmussen A, Lee S, Agaisse H (2013) The UPD3 cytokine couples environmental challenge and intestinal stem cell division through modulation of JAK/STAT signaling in the stem cell microenvironment. *Dev Biol* 373:383–393.